Front. Chem. Sci. Eng. 2022, 16(5): 745–754
https://doi.org/10.1007/s11705-021-2038-x

RESEARCH ARTICLE

Preparation of polysulfone-based block copolymer ultrafiltration membranes by selective swelling and sacrificing nanofillers

Shanshan Zhang[1], Jiemei Zhou[1], Zhaogen Wang[1], Jianzhong Xia (✉)[2,3], Yong Wang (✉)[1]

1 State Key Laboratory of Materials-Oriented Chemical Engineering, College of Chemical Engineering, Nanjing Tech University, Nanjing 211816, China
2 Institute for Advanced Study, Shenzhen University, Shenzhen 518060, China
3 Beijing OriginWater Membrane Technology Co., Ltd., Beijing 101407, China

Abstract Selective swelling of block copolymers of polysulfone-*b*-poly(ethylene glycol) is an emerging strategy to prepare new types of polysulfone ultrafiltration membranes. Herein, we prepared nanoporous polysulfone-*b*-poly(ethylene glycol) ultrafiltration membranes by selective swelling and further promoted their porosity and ultrafiltration performances by using $CaCO_3$ nanoparticles as the sacrificial nanofillers. Different contents of $CaCO_3$ nanoparticles were doped into the solution of polysulfone-*b*-poly(ethylene glycol), and thus obtained suspensions were used to prepare both self-supported and bi-layered composite structures. Selective swelling was performed on the obtained block copolymer structures in the solvent pair of ethanol/acetone, producing nanoporous membranes with poly(ethylene glycol) lined along pore walls. The $CaCO_3$ nanoparticles dispersed in polysulfone-*b*-poly(ethylene glycol) were subsequently etched away by hydrochloric acid and the spaces initially occupied by $CaCO_3$ provided extra pores to the block copolymer layers. The porosity of the membranes was increased with increasing $CaCO_3$ content up to 41%, but further increase in the $CaCO_3$ content led to partial collapse of the membrane. The sacrificial $CaCO_3$ particles provided extra pores and enhanced the connectivity between adjacent pores. Consequently, the membranes prepared under optimized conditions exhibited up to 80% increase in water permeance with slight decrease in rejection compared to neat membranes without the use of sacrificial $CaCO_3$ particles.

Keywords block copolymers, selective swelling ultrafiltration, $CaCO_3$ nanoparticles, sacrificial nanofillers

Received November 13, 2020; accepted January 8, 2021

E-mails: xiajianzhong@outlook.com (Xia J), yongwang@njtech.edu.cn (Wang Y)

1 Introduction

Ultrafiltration membranes with the typical pore size of 5–100 nm have been extensively used to remove colloids, organic contaminants, macromolecules and viruses in the field of wastewater treatment, water remediation, food processing, protein separation, gene engineering and so on [1–5]. Polysulfone (PSF) is one of the most commonly used commodity polymeric materials for the preparation of ultrafiltration membranes owing to the superior membrane-forming ability, excellent thermal stability and mechanical strength [6–8]. However, the intrinsic hydrophobicity of PSF brings the drawbacks of relatively low permeability and poor fouling resistance [9–11]. To address this issue, researchers have made tremendous efforts to tailor the surface property of PSF membranes to ensure better performances [12,13]. Typically, surface hydrophilic modification by chemical bonding or physical blending has been proved to be efficient ways to improve the permeance and simultaneously enhance the anti-fouling ability [14–16].

With respect to the hydrophilic modifiers, poly(ethylene glycol) (PEG) and PEG-containing copolymers have been widely used because of the nonionic character, high hydration capability and protein resistance of PEG [16–19]. For example, Mayes et al. used PSF-g-PEG as the additive and blended it with PSF to prepare ultrafiltration membranes [6]. Owing to the enrichment of PEG chains during the phase inversion process to generate porous structure, the hydrophilic surface was obtained on the produced PSF membranes, resulting in enhanced wettability and resistance to protein adsorption. Besides, diverse chemical modifications such as bioinspired adhesion via polydopamine and surface covalent grafting have also frequently been applied to anchor PEG chains onto the surface of PSF membranes to pursue high hydrophilicity

[6,20]. Distinct from above mentioned methods, our group adopted the amphiphilic block copolymer (BCP) of PSF-*b*-PEG as the precursor material and prepared ultrafiltration membranes using the process of selective swelling a few years ago [21–23]. The thermodynamic incompatibility of PEG and PSF chains leads to the phase separation of the copolymer, producing uniform PEG microdomains homogeneously dispersed in the PSF matrix. By immersing as-prepared PSF-*b*-PEG films into a solvent selective to PEG followed by drying, the phase-separated PSF-*b*-PEG films could be converted to nanoporous membranes based on the different swelling behavior of the PSF phase and PEG phase in selective solvents. Importantly, simultaneous to the pore-forming process, the PEG chains spontaneously migrate to the pore walls, endowing the membranes with superior hydrophilicity and consequently enhanced water permeance and fouling resistance [24]. Compared to commonly used methods based on phase inversion of polymer solutions, this selective swelling strategy is featured by simplicity, less consumption of organic solvents, and high flexibility in tuning pore sizes and geometries, and has emerged as a new process to prepare ultrafiltration membranes with well-defined structures and potentially enhanced performances [25].

BCP membranes prepared by selective swelling typically exhibit a symmetrical porous structure and consequently exhibit a large resistance of mass transfer if they are directly used for filtration. We have developed a few strategies to reduce mass transfer, thus enhancing permeance. For example, instead of using self-supported membranes with large thicknesses, we built a thin layer of BCP on porous substrates to prepare thin-film composite membranes, exhibiting significantly improved permeability [26]. We are aware of the fact that increasing the porosity is another effective way to improve the water permeance of membranes by providing additional water paths thus lowering the mass transfer resistance. For instance, the preparation of mixed matrix membranes by adding dispersed inorganic nanoparticles such as silica [27], titanium [28,29], and zeolite molecular sieves to polymers [30,31] has been extensively explored. Using silica particles as additives for cellulose acetate, Arthanareeswaran et al. prepared organic–inorganic composite membranes by the non-solvent induced phase separation method [27].The result revealed that the incorporation of silica particles significantly improved the surface porosity and resulted in a great improvement in water permeance. Except for being used as additives, inorganic nanomaterials can also be used as sacrificial nanofillers in the membrane preparation process [32,33]. For example, Zhang et al. coated sulfonated polyetherketone with cardo groups onto the copper hydroxide nanostrand layer and then removed nanostrands with hydrochloric acid to form ultrathin anionic polymer membranes [33]. This membrane exhibited an ultrahigh water permeance compared to commercial membranes. Inspired by these works, we assume that adding sacrificial additives to the matrix of BCP membranes followed by removing them *via* chemical etching is an effective method to improve porosity of the membrane, thus achieving better water permeance. Compared with other inorganic nanomaterials, $CaCO_3$ nanoparticles are one of the most extensively used low-cost, commercially available nanofillers [34]. Its surface polarity and particle size can be well adjusted in their current manufacturing process [34]. These characteristics make $CaCO_3$ nanoparticles the desired sacrificial nanofillers to prepare polymer membranes with high porosity.

In this work, we fabricated nanoporous PSF-*b*-PEG membranes by selective swelling and further promoted their porosity and ultrafiltration performances by using $CaCO_3$ nanoparticles as the sacrificial nanofillers (Fig. 1). Selective swelling of $CaCO_3$-blended PSF-*b*-PEG membranes in ethanol/acetone solvent pair produced bicontinuous nanoporous structures. Then, the $CaCO_3$ nanoparticles dispersed in membranes were etched by hydrochloric acid and the spaces initially occupied by $CaCO_3$ were converted to extra pores. The produced membranes showed significant increase in water permeance at little expense of rejection compared to neat PSF-*b*-PEG membranes, demonstrating that the integration of selective swelling process and sacrificial nanoparticles doping is an effective way to upgrade the performances of PSF-based ultrafiltration membranes.

2 Experimental

2.1 Materials

The PSF-*b*-PEG with the polydispersity index of ca. 2.0 was provided by Nanjing Bangding. The molecular weight (M_w) of PSF-*b*-PEG is 79.1 kDa and the weight ratio of the PEG block in the copolymer is 21%. PSF-*b*-PEG was dried at 120 °C for 24 h prior to use. $CaCO_3$ nanoparticles with an average particle size of 40 nm were provided by Raicheng Warner Nanomaterials Co., Ltd. and were dried at 80 °C for 48 h before use. All the solvents including 1,2-dichloroethane ($>99.0\%$), acetone ($>99.5\%$), hydrochloric acid (36%–38%) were obtained from Shanghai Lingfeng Chemical Reagent Co., Ltd. Anhydrous ethanol ($>99.8\%$) and Acid Orange 7 ($>85\%$) were purchased from Aladdin. The macroporous polyvinylidene fluoride (PVDF) substrates with a diameter of 47 mm and an average pore size of 0.22 μm were purchased from Merck Millipore Ltd. Bovine serum albumin (BSA) (98%, M_w = 66 kDa) and phosphate buffered solution tablets were purchased from MP Biomedicals, LLC. Monodispersed 10-nm gold colloid was purchased from British Biocell International Limited. Dextrans from Leuconostoc spp. (M_w = 10, 40, 70 and 500 kDa) were provided by Sigma-Aldrich. Deionized water was used in all tests. All reagents were of analytical grade and used as received.

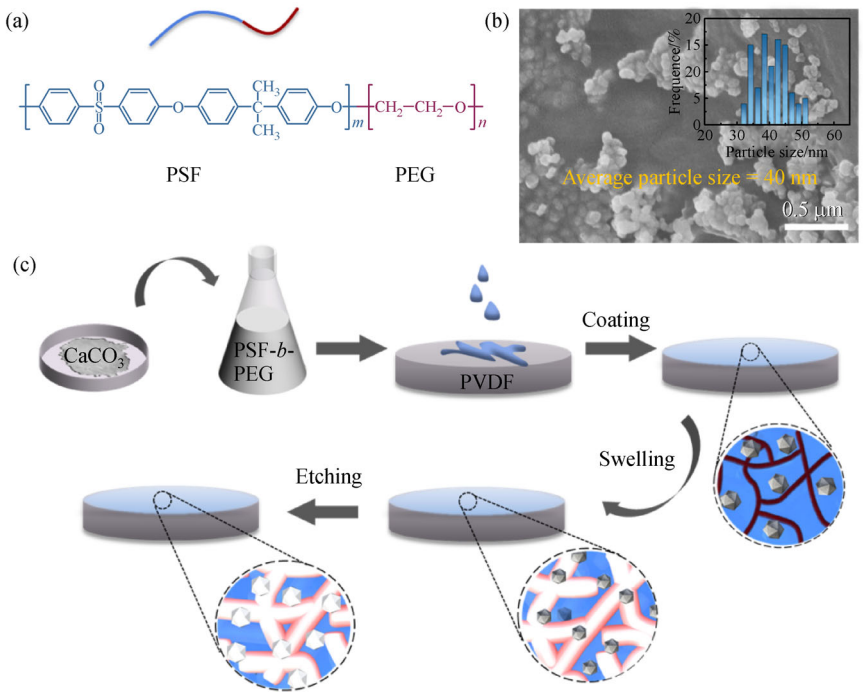

Fig. 1 (a) The structure formula of PSF-*b*-PEG; (b) the scanning electron microscope (SEM) image and particle size distribution of $CaCO_3$ nanoparticles; (c) the scheme for the preparation of PSF-*b*-PEG composite membranes by selective swelling and nanofillers etching.

2.2 Preparation of PSF-*b*-PEG membranes

We prepared two types of membranes: thick self-supported membranes and composite membranes with thin layers of PSF-*b*-PEG top-coated on porous substrates from 10 wt-% and 3 wt-% PSF-*b*-PEG solutions, respectively, containing $CaCO_3$ nanoparticles. PSF-*b*-PEG was dissolved in 1,2-dichloroethane to prepare the BCP solutions. The PSF-*b*-PEG solution was stirred (1500 $r \cdot min^{-1}$) at room temperature for over 2 h until the polymer was completely dissolved. A certain amount of $CaCO_3$ nanoparticles were added into the PSF-*b*-PEG solution, the mixture was sufficiently stirred to form homogenous suspension and then treated by ultrasonication for 10 min. The suspension with 10 wt-% PSF-*b*-PEG polymers was cast onto a clean glass plate with the casting knife preset to the height of 200 μm. The as-casted film was first dried at room temperature for 2 h, then placed in a 40 °C vacuum oven and dried for another 2 h. Finally, the temperature of oven was raised to 80 °C to dry the film thoroughly for 2 h. To cavitate the BCP thin film, selective swelling was firstly applied by immersing the film in acetone/ethanol solvent pair with the acetone content of 25% at 70 °C for 7 h. Then, the $CaCO_3$ nanoparticles in the film were etched by 10 wt-% hydrochloric acid. Afterwards, the produced membrane was rinsed with copious water for complete removal of salts. Finally, the self-supported PSF-*b*-PEG flat-sheet membrane was obtained after drying under ambient conditions.

The suspension with 3 wt-% PSF-*b*-PEG polymer was spin-coated onto a PVDF substrate after ultrasonification for 10 min to form a bi-layered composite membrane. This spin coating process was executed under a constant condition of 20 °C and 20% relative air humidity to eliminate the effects of temperature and humidity. Before coating, the PVDF substrate was soaked in deionized water for at least 20 min so that the macropores could be fully filled with deionized water to prevent the downward leakage of casting solution. The water-filled PVDF substrate was then placed on a clean glass slide and the remaining water on the surface was gently wiped with a filter paper. Then, the casting solution was spin-coated on the water-filled PVDF substrate. To cavitate the BCP layer, the composite membrane was immersed in acetone/ethanol solvent pair with the acetone content of 25% at 50 °C for 10 min. The next steps to remove $CaCO_3$ nanoparticles were the same as described above.

2.3 Characterizations

The field emission SEM (S-4800, Hitachi) was used to characterize the surface and cross-sectional morphologies with an acceleration voltage of 5.0 kV. Before characterization, all samples were sputter-coated with a thin layer of

gold to enhance their conductivity and avoid charging effects. The membrane was immersed in isopropyl alcohol for 10 min, then quick-frozen in liquid nitrogen and fractured to obtain the cross-sectional sample. At least 100 pores on the surface SEM images of each sample were measured to estimate the average pore sizes by using the software Nanomeasurer. An energy-dispersive X-ray (EDX) spectrometer (Noran) was used to analyze the Ca content of prepared membranes at an accelerating voltage of 30 kV.

The mass changes of the self-supported PSF-*b*-PEG membranes during treatments to generate pores were obtained by comparing the mass of corresponding samples. Mass loss (M, %) was calculated using Eq. (1):

$$M = \frac{M_O - M_E}{M_O} \times 100\%, \quad (1)$$

where M_O and M_E (g) are the masses of the original thin film and the membrane after swelling and etching, respectively. The thickness changes of membranes were recorded using a vernier caliper in dry state.

To measure the porosity, the flat-sheet membranes were immersed in deionized water, after 4 h soaking the water-filled membranes were taken out and carefully wiped using tissue paper to remove excess water on the surface. Then the wet membranes were weighed (ω_1, g), dried in the oven at 45 °C overnight, and re-weighed (ω_2, g). The water contents were calculated as ω_1–ω_2. The overall porosity (ε, %) was calculated using Eq. (2):

$$\varepsilon = \frac{\omega_1 - \omega_2}{\rho \times A \times l} \times 100\%, \quad (2)$$

where ρ (g·cm^{-3}) is the density of deionized water, l (cm) is membrane thickness, and A (cm^2) is the membrane area.

2.4 Filtration tests

The separation performances of PSF-*b*-PEG composite membranes were measured using a multi-cell cross-flow apparatus with a diameter of 3 cm. The filtration tests were operated at room temperature with a 600 r·min^{-1} stirring speed. In order to obtain a stable permeance, each membrane was subjected to compression at a pressure of 1 bar for 10 min, then the pure water permeance was measured at 1 bar. The water permeance (J_ω, L·m^{-2}·h^{-1}·bar^{-1}) was calculated via Eq. (3):

$$J_\omega = \frac{V}{A \times \Delta t \times p}, \quad (3)$$

where V (L) is the volume of pure water passing through the membrane within the testing time Δt, A (m^2) is the effective testing area of the membrane, and p (bar) is the testing pressure.

The aqueous solution of monodisperse gold colloids with a diameter of 10 nm was used to carry out the rejection tests. Rejection tests were performed at 1 bar and the flow velocity was maintained at 10 L·h^{-1}. To avoid any adsorption of gold nanoparticles on the membrane surface, the composite membranes were pretreated with the acid orange 7 solution (5 mg·L^{-1}) for 20 min to neutralize the surface before rejection testing [35]. The gold concentrations in feed, permeation and retentate were analyzed by the Ultraviolet-visible (UV-vis) absorption spectrometer at ca. 520 nm. The rejection rate of gold colloid nanoparticles (R_1, %) was calculated according to Eq. (4):

$$R_1 = \left(1 - \frac{C_P}{C_F}\right) \times 100\%, \quad (4)$$

where C_P (g·L^{-1}) and C_F (g·L^{-1}) are the concentrations of gold nanoparticles in the permeation and feed solutions, respectively.

BSA was dissolved in a phosphate buffered solution at a concentration of 0.5 g·L^{-1}. Then the BSA solution was used as feed solution to conduct the rejection tests of composite membranes. The BSA concentrations in feed and retentate were measured by UV-Vis absorption spectrometry at ca. 280 nm. The BSA rejection (R_2, %) was obtained via Eq. (5):

$$R_2 = \left(1 - \frac{C_P}{C_F}\right) \times 100\%, \quad (5)$$

where C_P (g·L^{-1}) and C_F (g·L^{-1}) are the concentrations of BSA in the permeation and feed solutions, respectively.

The mixed dextran solution was used to determine the molecular weight cut-off (MWCO) of the composite membranes. The mixed dextran solution was prepared by dissolving four kinds of dextran with different molecular weights (10, 40, 70, and 500 kDa) into 1 L deionized water. The concentration of each kind of dextran component was 2.5, 1, 1, and 2 g·L^{-1}, respectively. The dextran concentrations after filtration were determined by a gel permeation chromatograph (GPC, Waters 1515).

3 Results and discussion

3.1 Morphology evolution during swelling and etching

$CaCO_3$-containing self-supported PSF-*b*-PEG films were prepared by incorporating different amounts of $CaCO_3$ nanoparticles into PSF-*b*-PEG matrix as shown in Fig. S1 (cf. Electronic Supplementary Material, ESM). The original PSF-*b*-PEG films were transparent while the color of $CaCO_3$-containing PSF-*b*-PEG films gradually turned to white with increasing $CaCO_3$ content (Figs. S1 (a)–1(d)). The SEM observation revealed a smooth and non-porous structure of all the PSF-*b*-PEG films with or without incorporation of $CaCO_3$ nanoparticles (Fig. S2, cf. ESM). Following the process of selective swelling induced pore generation [36–38], the PSF-*b*-PEG films were

soaked with a selective solvent, acetone/ethanol solvent pair with the acetone content of 25%, at 70 °C for 7 h to form nanopores. Figure 2 and Fig. S3 (cf. ESM) showed the surface and cross-sectional SEM images of the self-supported PSF-*b*-PEG membranes prepared with different $CaCO_3$ contents. It can be seen that bi-continuous pores were formed on the surface (Figs. 2(a)–2(d)) and through the whole membrane thickness (Figs. S3(a)–3(d)) after swelling. The swelling-treated membranes (Figs. S1(e)–1(h)) became milky and opaque because of the abundant pores. During the swelling process, ethanol is preferentially enriched in PEG microdomains as it is a selective solvent to PEG [36], leading to volume expansion of PEG microdomains. Acetone is a selective solvent to PSF, and it helps to enhance the segmental mobility of the PSF chains because of the plasticization effect. The PSF matrix is subjected to local deformation driven by the expanding PEG microdomains. After withdrawing the membranes from swelling bath, ethanol and acetone evaporate and the volumes previously occupied by the swollen PEG chains are converted to pores [36]. According to our previous studies [15,22], both the formulation of solvent pair and swelling duration contribute to the porous structures of prepared membranes during the selective swelling process. We changed the mass ratio of acetone/ethanol in the swelling bath and the swelling durations to explore their effects on the morphologies of PSF-*b*-PEG membranes. SEM images of the self-supported PSF-*b*-PEG membranes under different swelling conditions were shown in Fig. S4 (cf. ESM). Upon swelling at 70 °C for 7 h, with the increase of acetone content from 20% to 25%, the surfaces of membranes gradually changed from a relatively dense skin layer (Fig. S4(a)) to a bi-continuous porous structure (Fig. S4(b)). However, when the acetone content was further increased to 30%, the strong swelling affinity for PSF matrix led to the micellization of BCP (Fig. S4(c)). Extending the swelling duration to 8 h also caused the micellization of PSF-*b*-PEG membranes (Figs. S4(d)–4(f)) subjected to swell with different acetone content (20%–30%), which is undesired for the separation applications. Therefore, all selective swelling processes were conducted in the swelling bath with 25% acetone content at 70 °C for 7 h in subsequent experiments unless specified otherwise.

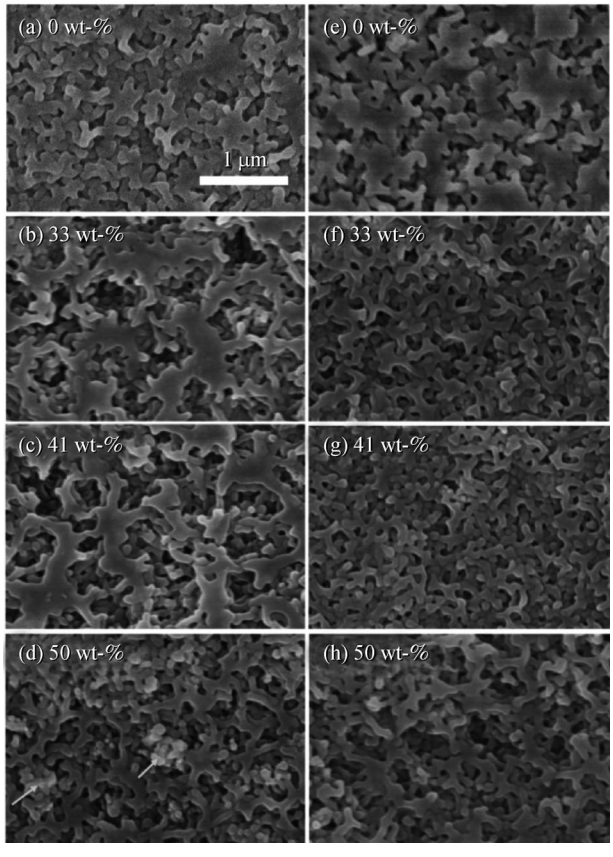

Fig. 2 SEM surface images of the self-supported PSF-*b*-PEG membranes prepared with different $CaCO_3$ contents after (a–d) swelling and (e–h) etching. The images are in the same magnification, and the scale bar corresponding to 1 μm is given in (a).

Although significant percentages of $CaCO_3$ nanoparticles were doped in PSF-*b*-PEG membranes, they can hardly be distinguished from the swelling-treated membranes (Figs. 2(b) and 2(c)). Only at the content of 50%, agglomeration of $CaCO_3$ nanoparticles can be occasionally observed (highlighted by the arrow in Fig. 2(d)). This is because $CaCO_3$ nanoparticles possess a size close to the feature size of the pores and the veins in the nanoporous membranes prepared by selective swelling. We then used EDX analysis to examine the distribution of Ca element on the membrane surface (Fig. 3). It can be seen from Figs. 3(a) and 3(d) that the Ca element marked as the red spots was uniformly distributed on the surface and cross-section of the membrane, and the Ca content was tested to be about 5% (Table. S1, cf. ESM) according to the result of EDX spectra (Fig. 3(b)). The surface concentration of Ca was slightly higher than the Ca concentration in the bulk membrane. To further promote porosity, $CaCO_3$ nanoparticles were etched by 10 wt-% hydrochloric acid. After etching, the peak of Ca element on the EDX spectrum completely disappeared (Figs. 3(c) and 3(f)), and the Ca content was proved to be 0% (Table S1), demonstrating $CaCO_3$ nanoparticles were thoroughly removed. The membranes preserved the bi-continuous porous structure (Figs. 2(e)–2(h)). However, the porosity change after etching treatment cannot be seen directly from the SEM images.

3.2 The changes in membrane mass and porosity

The masses of the original membranes, and the membranes after swelling and etching were recorded, and the mass losses of the self-supported PSF-*b*-PEG membranes with different $CaCO_3$ contents were calculated and compared. As shown in Fig. 4, the mass of the membrane without loading $CaCO_3$ nanoparticles had almost no change after

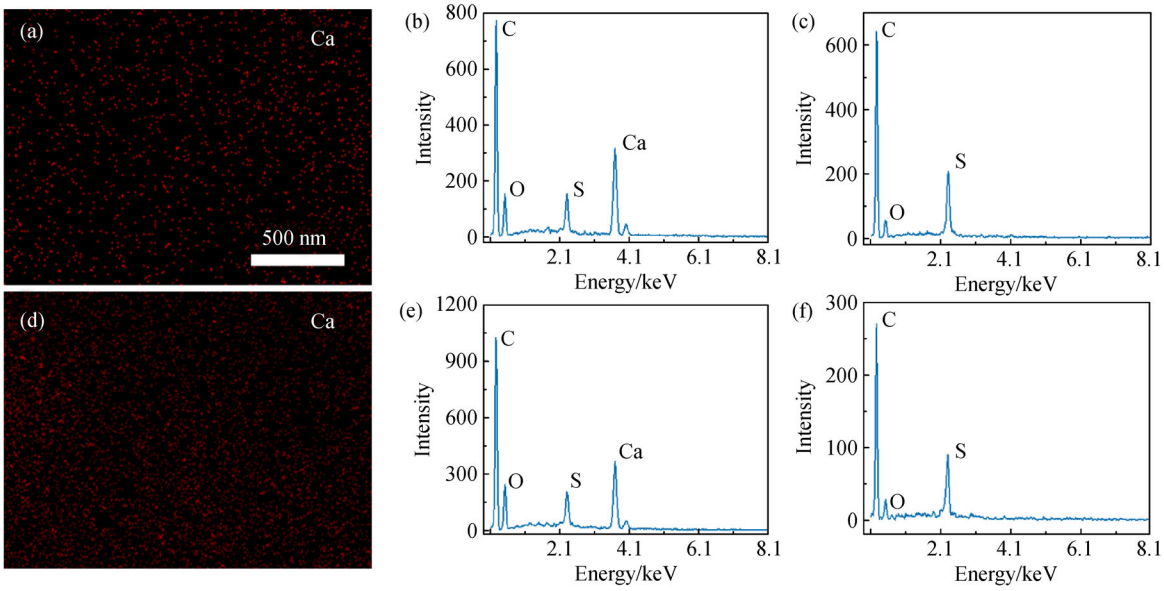

Fig. 3 (a) Surface and (d) cross-sectional EDX images of the self-supported PSF-*b*-PEG membrane prepared with 50% $CaCO_3$ before etching. EDX spectra of the self-supported PSF-*b*-PEG membrane prepared with 50% $CaCO_3$: (b and e) before and (c and f) after etching. The images are in the same magnification, and the scale bar corresponding to 500 nm is given in (a).

swelling and etching. With the increase of $CaCO_3$ contents doped in membranes from 0%, 9%, 17%, 33%, 41% to 50%, the mass losses of membranes during swelling and etching increased linearly and matched the initial $CaCO_3$ content well, demonstrating that $CaCO_3$ nanoparticles were completely removed by hydrochloric acid which is consistent with the EDX analysis.

We evaluated the thicknesses and porosities of the self-supported PSF-*b*-PEG membranes with different $CaCO_3$ contents. As shown in Fig. 5, with increasing $CaCO_3$ content, the thicknesses of the original PSF-*b*-PEG films before swelling increased due to the increasing total concentration of casting solution. After swelling treatment, the thicknesses of the membranes further increased compared to the original films while the increments were not dependent on the contents of $CaCO_3$ (Fig. 5(a)). The selective swelling is a physical pore-forming process and has no chemical destruction to the membrane. In the process of swelling, the PSF-*b*-PEG membrane experiences a significant volume expansion as a large number of pores are formed without sacrificing any chemical component of the BCP. The volume expansion causes the membrane to deform in the direction perpendicular to the membrane surface, that is, the membrane thickness increases. Therefore, the increase in membrane thickness depends on the swelling conditions and the $CaCO_3$ content is irrelevant for the swelling behavior.

As shown in Fig. 5(b), the porosity of the membrane prepared without loading $CaCO_3$ was 44%, and the porosities of the membranes with 17%, 33%, 41% and 50% $CaCO_3$ loading were 50%, 61%, 66%, and 47%, respectively. Apparently, the sacrificial $CaCO_3$ helped to improve the overall porosities of membranes. The doped $CaCO_3$ nanoparticles have an average particle size of 40 nm according to the SEM characterization (Fig. 1(b)), which is close to the diameter of the pores in the membranes formed by selective swelling. When the added $CaCO_3$ nanoparticles were removed, the positions occupied by the $CaCO_3$ were left, thereby forming vacancies replicating the size of $CaCO_3$ nanoparticle. However, once an overdose of $CaCO_3$ was used, the porosity showed no further increase but began to decrease, which is because the large amount of pores created by removing $CaCO_3$ would adversely affect the structural

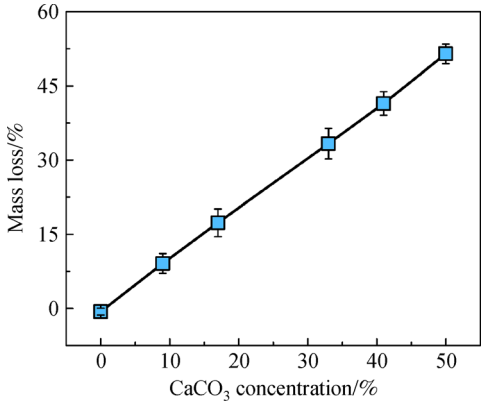

Fig. 4 Mass changes of the self-supported PSF-*b*-PEG membranes with different $CaCO_3$ concentrations after etching with hydrochloric acid.

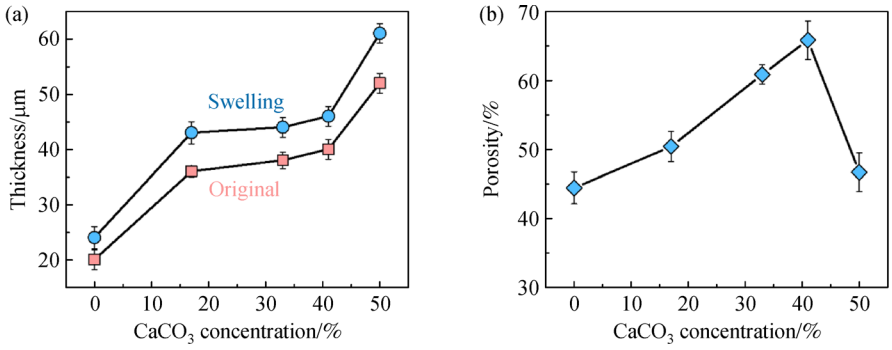

Fig. 5 (a) Thicknesses and (b) porosities of the self-supported PSF-*b*-PEG membranes prepared with different $CaCO_3$ concentrations.

stability of membranes and result in the collapse of the PSF-*b*-PEG matrix. When the content of $CaCO_3$ doped was 41%, the membrane achieved the highest porosity of 66%.

3.3 Ultrafiltration performances of composite membranes

The self-supported PSF-*b*-PEG flat-sheet membrane has a symmetrical structure and relatively large thickness, which always leads to a low water flux. In order to prepare membranes with better separation performance for ultrafiltration, we lowered the PSF-*b*-PEG concentration to 3 wt-%, and spin-coated the suspensions of PSF-*b*-PEG and different contents of $CaCO_3$ in 1,2-dichloroethane on macroporous PVDF substrates. After swelling and etching treatment, the composite membranes composed of the nanoporous BCP separation layers and the supporting PVDF substrates were formed (Fig. 6). The BCP layer showed a bi-continuous pore morphology with a thickness of 480 nm as shown in Figs. 6(a) and 6(b). The pure water permeances of the composite membranes were tested. As shown in Fig. 6(c), the permeance of the membrane prepared without loading $CaCO_3$ was 196 $L \cdot m^{-2} \cdot h^{-1} \cdot bar^{-1}$, and the permeances of the membranes with 23%, 33%, 41% and 50% $CaCO_3$ loading were 253, 300, 353, and 273 $L \cdot m^{-2} \cdot h^{-1} \cdot bar^{-1}$, respectively. It can be seen that the pure water permeances were increased first and then decreased with the rising $CaCO_3$ contents, which is exactly in tune with the porosity change of self-supported PSF-*b*-PEG membranes shown in Fig. 5(b). Considering the porosity of self-supported PSF-*b*-PEG membranes could be reflective of the porosity of PSF-*b*-PEG layers in composite membranes, it can be said that the water permeance of the composite membrane depends closely to the porosity of PSF-*b*-PEG layers. The permeance increase is because that the increased $CaCO_3$ loading in the casting solution leads to more pores in the PSF-*b*-PEG layer of the prepared composite membrane, increases the porosity, and also make the pores produced by selective swelling more interconnected, which apparently reduces the mass transfer resistance for water transportation during filtration. Nevertheless, the collapse of the PSF-*b*-PEG layer at a higher $CaCO_3$ content of 50% results in growing mass transfer resistance, thus decreasing the permeance. The pure water permeance could reach a highest value of 353 $L \cdot m^{-2} \cdot h^{-1} \cdot bar^{-1}$ at a $CaCO_3$ content of 41%, which was significantly improved by 80% compared with the permeance of the membrane without loading $CaCO_3$.

The MWCOs of PSF-*b*-PEG composite membranes fabricated with the different contents of $CaCO_3$ were determined by testing the rejections to dextrans with varied molecular weights (Fig. S6, cf. ESM). The MWCO of the membrane fabricated without loading $CaCO_3$ was determined to be 52000 Da, and the MWCOs of membranes prepared with 23%, 33%, 41% and 50% $CaCO_3$ concents were all close to 63000 Da (Fig. S6, cf. ESM). According to the Stokes-Einstein radius of dextrans [39,40], the effective pore sizes in the separation layer of the membranes prepared with or without incorporation of $CaCO_3$ were estimated to be 9.7 and 10.6 nm. We know that the pores created by selective swelling and by removing the $CaCO_3$ nanoparticles were around 40 nm, which are much larger than the calculated pore sizes. This is because the membranes for SEM were in the dry state and the hydrophilic PEG chains were collapsed on the PSF matrix in this case, while the PEG chains were in an extended conformation when the membrane is used in water. Therefore, the effective pore size of the membrane in water systems was smaller than that observed from SEM. Moreover, the MWCO tests reveal that the $CaCO_3$ loading leads a minor increase of the effective pore size of the PSF-*b*-PEG composite membrane while the $CaCO_3$ contents varied from 23% to 50% have little effect on the pore size.

Two model materials including BSA and monodispersed gold nanoparticles were used to probe the size-sieving separation capability of the membranes. As can be seen from Fig. 6(d), the membrane prepared without loading $CaCO_3$ showed a high rejection of 97% to 10 nm gold nanoparticles. As the $CaCO_3$ content was increased to 23%, 33%, 41% and 50%, the rejections were determined to be 96%, 96%, 94% and 95%, respectively. Figure 6(f)

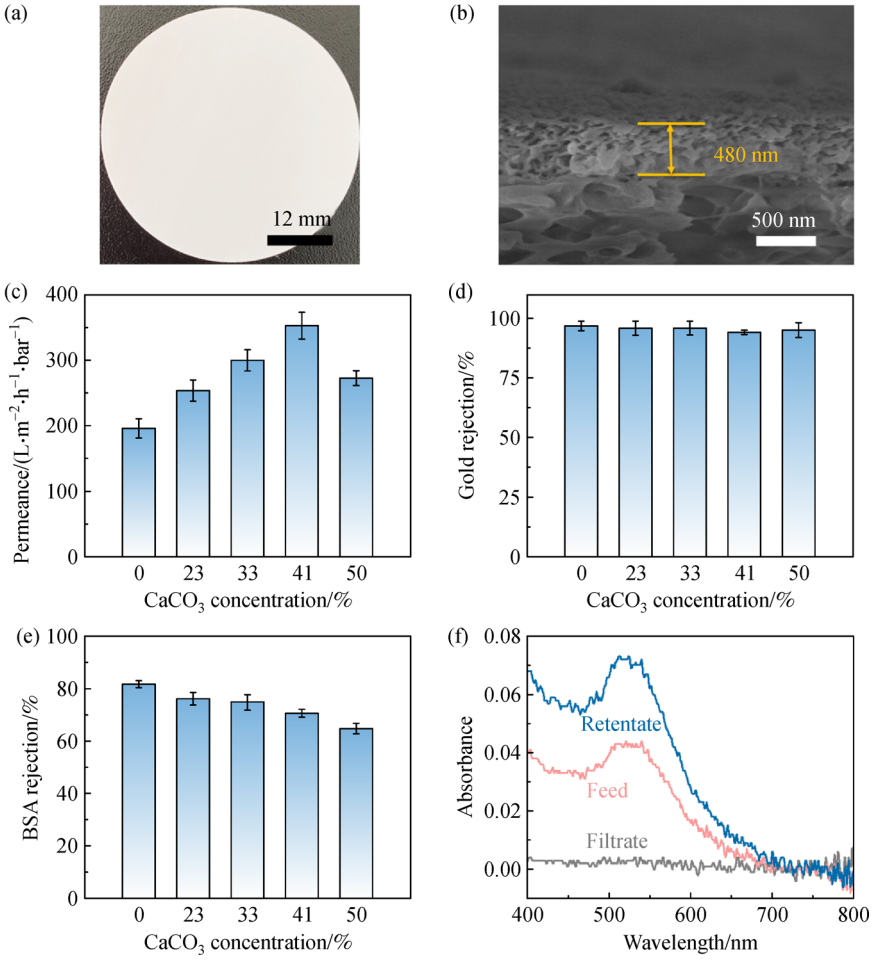

Fig. 6 (a) The photograph and (b) the cross-sectional SEM image of the PSF-*b*-PEG composite membrane. Permeance and rejection performances of membranes prepared with different $CaCO_3$ concentrations: (c) pure water permeance; (d) rejection to 10-nm gold nanospheres; (e) BSA rejection. (f) UV-vis absorption spectra of the feed, filtrate and retentate solutions of 10-nm gold nanoparticles through the PSF-*b*-PEG composite membrane prepared with 41% $CaCO_3$.

shows UV-vis absorption spectra of the feed, filtrate and retentate of 10 nm gold nanoparticles by using the composite membrane prepared with 41% $CaCO_3$. The characteristic peak of gold nanoparticles at 520 nm almost disappeared in the filtrate. Meanwhile, the absorbance in the retentate was intensified significantly, indicating that the rejection of the membrane was due to the size-sieving effect rather than the adsorption effect. Generally, the membranes maintained the high rejections to 10 nm gold nanoparticles in spite of the $CaCO_3$ content, which is coincident with MWCO results.

The gold nanoparticles are in the spherical shape, comparatively easy to be intercepted by the bi-continuous pores in the BCP layers. Herein, the separation performance to BSA, which is in an ellipsoidal shape with the size of 14 nm × 3.8 nm × 3.8 nm and a hydrodynamic diameter of ca. 7.2 nm, was also tested. As can be seen from Fig. 6(e), the BSA rejection of the membrane was 82%, which is lower than the rejection to gold nanoparticle resulted from the smaller hydrodynamic diameter of BSA, when no $CaCO_3$ nanoparticles were loaded. The incorporation with $CaCO_3$ as the sacrificial nanofillers in the membrane led to the decrease of the rejection as a result of enlarged pore size. With the increase of $CaCO_3$ loading from 23% to 33%, 41%, and 50%, the BSA rejection was slightly decreased from 76% to 75%, 71%, and 65%, respectively, although the effective pore sizes of membranes were barely changed. This can be understood that for the anisotropic BSA molecules, the increased porosity has more chance to allow them percolate through the pores by changing their orientation toward the pores during the rejection tests, leading to decreased retentions. For the $CaCO_3$ loading of 50%, the collapse of PSF-*b*-PEG matrix may cause opposite effect on the integrity of the porous structure of the membrane, therefore, the BSA rejection was further decreased although the porosity was not increased.

Overall, the permeances of the PSF-*b*-PEG composite

membranes can be significantly improved by adjusting the added $CaCO_3$ content, meanwhile, the membranes are able to keep a high rejection to 10 nm gold nanoparticles and a moderate rejection to BSA. Under the optimal condition of 41% $CaCO_3$ content, the membrane exhibits a pure water permeance of 350 $L \cdot m^{-2} \cdot h^{-1} \cdot bar^{-1}$ and the rejections to 10 nm gold nanoparticles and BSA are 94% and 71%, respectively.

4 Conclusions

In summary, we fabricated nanoporous PSF-*b*-PEG membranes based on selective swelling induced pore generation and further promoted their porosity and ultrafiltration performances by using $CaCO_3$ nanoparticles as the sacrificial nanofillers. The PSF-*b*-PEG polymer solution was blended with different contents of $CaCO_3$ nanoparticles and then used for the membrane preparation. First by immersing into the ethanol/acetone paired solvents for certain duration, the bi-continuous porous structure was produced following the mechanism of selective swelling-induced pore generation. Subsequent etching the $CaCO_3$ nanoparticles embedded in the PSF-*b*-PEG matrix provided extra vacancies, thus improving the porosity further. The increase of $CaCO_3$ content from 0% to 23%, 33%, 41% led to the significant raising of porosity while the porosity began to decrease at the $CaCO_3$ content of 50%, which was due to the collapse of the porous structures. At a $CaCO_3$ content of 41%, the water permeance of the PSF-*b*-PEG composite membrane was increased by 80% while the rejection was only slightly reduced compared to the membrane without $CaCO_3$ loading. This was because the extra pores resulted from sacrificial $CaCO_3$ particles had similar sizes with the pores from selective swelling, and they could provide additional channels for water but scarcely affected the rejection. It should be noted that such an ultrafiltration performance can also be obtained from membranes prepared by commonly used process of non-solvent induced phase separation, however, the performances of the membranes prepared by our newly emerged strategy is expected to be further improved by optimizing the preparation parameters and by designing new structures, for example, reducing the thickness of the BCP selective layer or building asymmetric porosity in this layer.

Acknowledgements Financial support from the National Natural Science Foundations of China (Grant Nos. 21776126 and 21825803) are gratefully acknowledged. We also thank the support from the Program of Excellent Innovation Teams of Jiangsu Higher Education Institutions and the Project of Priority Academic Program Development of Jiangsu Higher Education Institutions.

Electronic Supplementary Material Supplementary material is available in the online version of this article at https://dx.doi.org/10.1007/s11705-021-2038-x and is accessible for authorized users.

References

1. Amanda A, Kulprathipanja A, Toennesen M, Mallapragada S K. Semicrystalline poly(vinyl alcohol) ultrafiltrationmembranes for bioseparations. Journal of Membrane Science, 2000, 176(1): 87–95
2. Lee A, Elam J W, Darling S B. Membrane materials for water purification: design, development, and application. Environmental Science. Water Research & Technology, 2016, 2(1): 17–42
3. Castro-Muñoz R, Boczkaj G, Gontarek E, Cassano A, Fíla V. Membrane technologies assisting plant-based and agro-food by-products processing: a comprehensive review. Trends in Food Science & Technology, 2020, 95: 219–232
4. Boulkrinat A, Bouzerara F, Harabi A, Harrouche K, Stelitano S, Russo F, Galiano F, Figoli A. Synthesis and characterization of ultrafiltration ceramic membranes used in the separation of macromolecular proteins. Journal of the European Ceramic Society, 2020, 40(15): 5967–5973
5. Premnath S, Agarwal G P. Single stage ultrafiltration for enhanced reverse selectivity in a binary protein system. Separation Science and Technology, 2017, 52(13): 2161–2172
6. Park J Y, Acar M H, Akthakul A, Kuhlman W, Mayes A M. Polysulfone-graft-poly(ethylene glycol) graft copolymers for surface modification of polysulfone membranes. Biomaterials, 2006, 27(6): 856–865
7. Yang Y N, Zhang H X, Wang P, Zheng Q Z, Li J. The influence of nano-sized TiO_2 fillers on the morphologies and properties of PSF UF membrane. Journal of Membrane Science, 2007, 288(1-2): 231–238
8. Zodrow K, Brunet L, Mahendra S, Li D, Zhang A, Li Q L, Alvarez P J J. Polysulfone ultrafiltration membranes impregnated with silver nanoparticles show improved biofouling resistance and virus removal. Water Research, 2009, 43(3): 715–723
9. Rana D, Matsuura T. Surface modifications for antifouling membranes. Chemical Reviews, 2010, 110(4): 2448–2471
10. Sheldon J M, Reed I M, Hawes C R. The fine-structure of ultrafiltration membranes. 2. Protein fouled membranes. Journal of Membrane Science, 1991, 62(1): 87–102
11. Mauter M S, Wang Y, Okemgbo K C, Chinedum O O, Giannelis E P, Elimelech M. Antifouling ultrafiltration membranes via post-fabrication grafting of biocidal nanomaterials. ACS Applied Materials & Interfaces, 2011, 3(8): 2861–2868
12. Chen Y Q, Wei M J, Wang Y. Upgrading polysulfone ultrafiltration membranes by blending with amphiphilic block copolymers: beyond surface segregation. Journal of Membrane Science, 2016, 505: 53–60
13. Wang N, Wang T, Hu Y X. Tailoring membrane surface properties and ultrafiltration performances via the self-assembly of polyethylene glycol-block-polysulfone-block-polyethylene glycol block copolymer upon thermal and solvent annealing. ACS Applied Materials & Interfaces, 2017, 9(36): 31018–31030
14. Wang Z G, Yao X P, Wang Y. Swelling-induced mesoporous block copolymer membranes with intrinsically active surfaces for size-selective separation. Journal of Materials Chemistry, 2012, 22(38): 20542–20548
15. Guo L M, Wang Z G, Wang Y. Selective swelling of block

copolymers for porous nanostructures. World Scientific Reference of Hybrid Materials, 2018, 1(15): 45–118
16. Zhao W, Su Y L, Li C, Shi Q, Ning X, Jiang Z Y. Fabrication of antifouling polyethersulfone ultrafiltration membranes using Pluronic F127 as both surface modifier and pore-forming agent. Journal of Membrane Science, 2008, 318(1-2): 405–412
17. Wang S F, Feng J Y, Xie Y, Tian Z Z, Peng D D, Wu H, Jiang Z Y. Constructing asymmetric membranes via surface segregation for efficient carbon capture. Journal of Membrane Science, 2016, 500: 25–32
18. Zhao Y F, Zhang P B, Sun J, Liu C J, Zhu L P, Xu Y Y. Electrolyte-responsive polyethersulfone membranes with zwitterionic polyethersulfone-based copolymers as additive. Journal of Membrane Science, 2016, 510: 306–313
19. Hancock L F, Fagan S M, Ziolo M S. Hydrophilic, semipermeable membranes fabricated with poly(ethylene oxide)-polysulfone block copolymer. Biomaterials, 2000, 21(7): 725–733
20. Du R K, Gao B J, Li Y B. Hydrophilic polysulfone film prepared from polyethylene glycol monomethylether via coupling graft. Applied Surface Science, 2013, 274: 288–294
21. Wang Y. Nondestructive creation of ordered nanopores by selective swelling of block copolymers: toward homoporous membranes. Accounts of Chemical Research, 2016, 49(7): 1401–1408
22. Yan N N, Wang Y. Selective swelling induced pore generation of amphiphilic block copolymers: the role of swelling agents. Journal of Polymer Science. Part B, Polymer Physics, 2016, 54(9): 926–933
23. Wang Y, Li F B. An emerging pore-making strategy: confined swelling-induced pore generation in block copolymer materials. Advanced Materials, 2011, 23(19): 2134–2148
24. Shar J A, Obey T M, Cosgrove T. Adsorption studies of polyethers. Part 1. Adsorption onto hydrophobic surfaces. Colloids and Surfaces. A, Physicochemical and Engineering Aspects, 1998, 136 (1-2): 21–33
25. Zhou J M, Wang Y. Selective swelling of block copolymers: an upscalable greener process to ultrafiltration membranes? Macromolecules, 2020, 53(1): 5–17
26. Yang H, Zhou J M, Wang Z G, Shi X S, Wang Y. Selective swelling of polysulfone/poly(ethylene glycol) block copolymer towards fouling-resistant ultrafiltration membranes. Chinese Journal of Chemical Engineering, 2020, 28(1): 98–103
27. Arthanareeswaran G, Sriyamuna Devi T K, Raajenthiren M. Effect of silica particles on cellulose acetate blend ultrafiltration membranes: Part I. Separation and Purification Technology, 2008, 64(1): 38–47
28. Emadzadeh D, Lau W J, Matsuura T, Ismail A F, Rahbari-Sisakht M. Synthesis and characterization of thin film nanocomposite forward osmosis membrane with hydrophilic nanocomposite support to reduce internal concentration polarization. Journal of Membrane Science, 2014, 449: 74–85
29. Emadzadeh D, Lau W J, Matsuura T, Rahbari-Sisakht M, Ismail A F. A novel thin film composite forward osmosis membrane prepared from PSf-TiO_2 nanocomposite substrate for water desalination. Chemical Engineering Journal, 2014, 237: 70–80
30. Ma N, Wei J, Qi S, Zhao Y, Gao Y B, Tang C Y Y. Nanocomposite substrates for controlling internal concentration polarization in forward osmosis membranes. Journal of Membrane Science, 2013, 441: 54–62
31. Lai L L, Shao J, Ge Q Q, Wang Z B, Yan Y S. The preparation of zeolite NaA membranes on the inner surface of hollow fiber supports. Journal of Membrane Science, 2012, 409–410: 318–328
32. Vilakati G D, Wong M C Y, Hoek E M V, Mamba B B. Relating thin film composite membrane performance to support membrane morphology fabricated using lignin additive. Journal of Membrane Science, 2014, 469: 216–224
33. Deng C, Zhang Q G, Han G L, Gong Y, Zhu A M, Liu Q L. Ultrathin self-assembled anionic polymer membranes for superfast size-selective separation. Nanoscale, 2013, 5(22): 11028–11034
34. Liu H Y, Liu L L, Yang C L, Li Z H, Xiao Q Z, Lei G T, Ding Y H. A hard-template process to prepare three-dimensionally macroporous polymer electrolyte for lithium-ion batteries. Electrochimica Acta, 2014, 121: 328–336
35. Uchida E, Uyama Y, Ikada Y. Zeta potential of polycation layers grafted onto a film surface. Langmuir, 1994, 10(4): 1193–1198
36. Wang Z G, Liu R, Yang H, Wang Y. Nanoporous polysulfones with in situ PEGylated surfaces by a simple swelling strategy using paired solvents. Chemical Communications, 2017, 53(65): 9105–9108
37. Darling S B. Directing the self-assembly of block copolymers. Progress in Polymer Science, 2007, 32(10): 1152–1204
38. Abetz V, Simon P F W. Phase behaviour and morphologies of block copolymers. Advances in Polymer Science, 2005, 189: 125–212
39. Aimar P, Meireles M, Sanchez V. A contribution to the translation of retention curves into pore size distributions for sieving membranes. Journal of Membrane Science, 1990, 54(3): 321–338
40. Calvo J I, Peinador R I, Prádanos P, Palacio L, Bottino A, Capannelli G, Hernández A. Liquid–liquid displacement porometry to estimate the molecular weight cut-off of ultrafiltration membranes. Desalination, 2011, 268(1-3): 174–181